Physical Integration of a Photovoltaic-Battery System
A Thermal Analysis

Vega Garita, Victor; Ramirez Elizondo, Laura; Bauer, Pavol

DOI
10.1016/j.apenergy.2017.10.007

Publication date
2017

Document Version
Final published version

Published in
Applied Energy

Applied Energy 208 (2017) 446–455

Contents lists available at ScienceDirect

Applied Energy

journal homepage: www.elsevier.com/locate/apenergy

Physical integration of a photovoltaic-battery system: A thermal analysis

Victor Vega-Garita*, Laura Ramirez-Elizondo, Pavol Bauer

DC Systems, Energy Conversion and Storage at Delft University of Technology, P.O. Box 5031, 2600 GA Delft, Netherlands

HIGHLIGHTS

- The thermal analysis proves the feasibility of the integration concept.
- The battery pack never surpasses the highest temperature of operation.
- Phase change material decreases the maximum battery temperature by 5 °C.
- The experimental results on a prototype validate the thermal model.

GRAPHICAL ABSTRACT

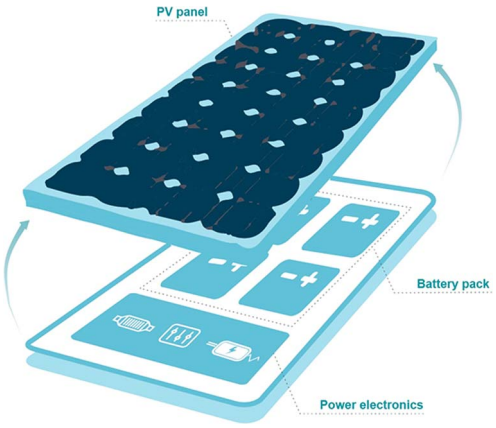

ARTICLE INFO

Keywords:
Solar-battery integration
Thermal analysis
Thermal management
Phase change materials
Finite element method

ABSTRACT

Solar-battery systems are still expensive, bulky, and space consuming. To tackle these issues, we propose a novel device that combines all the components of a solar-battery system in one device. This device might help reduce installation cost compared to the current solar-battery systems as well as provide a *plug-and-play* solution. However, this physical integration means higher temperatures for the components. Therefore, this paper presents a thermal analysis of the physical integration concept to evaluate its feasibility, focusing on the batteries, the most delicate components. The thermal analysis was conducted using a Finite Element Method model and validated with experimental results on a prototype. According to the model, the temperature of the components (battery and converters) reduced drastically by adding an air gap of 5–7 cm between the solar panel and the components. Even under severe conditions, maximum battery temperature never surpassed the highest temperature of operation defined by the manufacturer. Moreover, the maximum battery temperature decreases even further by applying a phase change material as a passive cooling method, reducing it by 5 °C. As a result, the battery pack operates in a safe range when combined with a 265 W_p solar panel, demonstrating the potential of this concept for future solar-battery applications.

1. Introduction

The power produced by a photovoltaic (PV) panel depends on several environmental conditions. A change in either irradiance or ambient temperature, for instance, results in fluctuations of the output power. Therefore, PV panels are not a stable energy source, posing many challenges. A possible solution to cope with these fluctuations is to couple PV panels with energy storage devices. For residential load

* Corresponding author.
E-mail address: v.e.vegagarita@tudelft.nl (V. Vega-Garita).

http://dx.doi.org/10.1016/j.apenergy.2017.10.007
Received 5 June 2017; Received in revised form 15 September 2017; Accepted 2 October 2017
Available online 21 October 2017

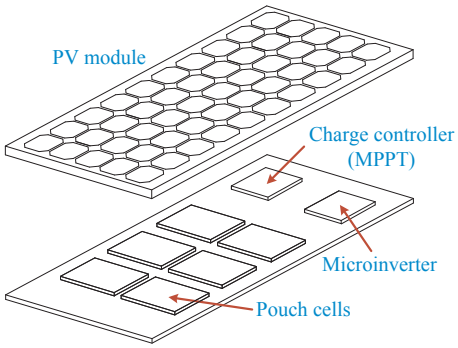

Fig. 1. PV-Battery Integrated Module concept.

levels, batteries are part of PV-storage systems because of their stability, reasonable price, low maintenance cost, and maturity. They provide energy when there is no solar generation, or store energy during moments of high solar generation for later use.

Despite the fact that PV panels and batteries prices are dropping fast [1,2], PV-Battery systems are still expensive. Current PV-Battery systems are complex to design and install. They require extensive technical advice and labour to build the system, impacting the total system cost. In a typical PV-Battery system, PV panels on the roof are usually connected to the power electronics and batteries separately inside the households, making the installation process complicated and time-consuming. The installation cost of solar systems accounts for around 21% of the total cost when other soft costs, not related to hardware (taxes, profit, etc.), are considered [3].

In an effort to diminish costs and make PV-Battery systems more simple to install, one package including a PV panel and all the balance-of-systems components might result in an attractive solution for the solar energy market [4]. We propose a novel device that combines a battery, charge controller, microinverter, and a PV module in one device (refer to Fig. 1). This device, *PV-Battery Integrated Module* (*PBIM*), is developed to provide a modular *plug-and-play* solution for PV-systems' owners. The *PBIM* can be also utilized for portable solutions or as a building block for standalone systems.

1.1. Literature study

The physical integration of PV devices and storage has been explored previously [5–7]. Advances in mechanical properties of the solar cells and batteries have propitiated their incursion in low power wearable devices [8,9], while fiber-shape devices have been woven into textile [10–13]. The majority of these low power devices lack controllable charging and discharging processes, leading to inefficient solutions [14–17]. For this reason, power electronics is essential to operate the PV cells and batteries at their maximum capacity, in particular for medium-power applications, as intended in this paper.

Although some steps to integrate normal size PV panels (circa 200 W) and balance-of-system components have been reported [18,19], just a few papers have coupled batteries directly with solar panels in one device. A combination of PV panel, battery, and electronic control unit was initially suggested in [20], stating the different advantages, general restrictions, and operational conditions of the so-called *multi-functional module*. Following this, the battery management system was proposed [21], and later, this concept was designed to supply bigger loads. The construction, control, and testing of the prototype were presented in [22]. Moreover, the details of the construction and installation of an integrated module for portable applications were published in [23].

At the time of writing this article, we did not find any paper focusing on the thermal implications derived from the physical integration (PI). Nevertheless, a vast amount of previous papers have investigated the thermal behaviour of PV panel and batteries operating individually [24,25], finding that thermal management systems are necessary to decrease the impact on efficiency and safety [26]. Most of the active cooling solutions (e.g. air or liquid forced convection systems, heat pipe, thermoelectric devices, and cold pipe) are complex to implement and maintain, and therefore costly [27]. Additionally, active cooling consumes a portion of the power generated by the PV panels, decreasing the total efficiency of the system. Instead, phase change materials (PCM) have demonstrated to be a promising option as a passive thermal management system for PV panels and batteries [28]. In comparison to active cooling systems for batteries, PCM achieve higher temperature uniformity [29], prevent temperature peaks [30], provide temperature regulation [31], and keep battery operating under safe temperature thresholds [32]. These are the reasons behind the use of PCM in this study.

1.2. Contribution

While some researchers have developed similar ideas to integrate a PV-Battery system in one device, there are still several gaps to fill regarding the feasibility of the PI concept. In particular, a thorough understanding of the thermal processes that take place when integrating all the components together, and their implications to the battery pack. In this paper, we contribute towards

- build (Section 3) and validate (Section 5) a thermal model for the *PBIM* using the Finite Element Method (FEM),
- understand the effect of directly attaching the components to the PV panel (Section 4.1) or including an air gap between them (Section 4.2),
- estimate the maximum battery temperatures and PV temperatures reached under extreme conditions (Section 4.3),
- evaluate the effectiveness of including a phase change material as thermal management method (Section 4.4), and
- prove that batteries can operate in a safe temperature range, and *PBIM* is technically feasible for solar energy applications (Section 4.3).

2. Physical design

For an optimal design of the *PBIM*, the following criteria must be satisfied:

- Heat has to be dissipated efficiently to avoid overheating.
- The device must prevent the entrance of dust and water from the environment.
- The frame must hold the components to ensure they do not move when installing and operating.
- Total volume and weight of the *PBIM* should be reduced as much as possible.

Given the requirements, pouch cells or prismatic cells are preferred due to their thin profile; they help to achieve high packaging as well as notable storage energy capacity per unit of volume. This sort of cells also provides a more extended surface allowing better heat dissipation than other geometries.

For the model, fifteen $LiFePO_4$ cells (A123 AMP20) are used to store the energy coming from the PV panel (265 W_p from Jinko Solar). The PV panel was chosen after comparing several options, based on efficiency, weight, cost, and temperature coefficients.

Due to the fact that the integration concept is relatively new, the size of the components and other features are assumed similar to the commercial charge controllers and microinverters (see Table 2).

3. Finite element method model

Develop a model that includes the heat generated and dissipated to

Table 1
Parameters for the steady state simulation.

Parameters	Value	Parameters	Value
G	1050 W m^{-2}	$\dot{q}_{converter}$	4500 W m^{-3}
T_{amb}	35 °C	h_{top}	6 W m^{-2} K^{-1}
$\dot{q}_{battery}$	10,000 W m^{-3}	h_{bottom}	6 W m^{-2} K^{-1}

Table 2
Parameters used in the FEM model.

Constants	Description	Value
P_{rated}	Rated power of PV panel	265 W_p
T_{NOCT}	PV panel NOCT temperature	45 °C
L_{PV}	PV panel length	1.65 m
W_{PV}	PV panel width	1 m
$V_{OC,PV}$	Open circuit voltage PV panel	38.6 V
V_{mpp}	Maximum power point voltage PV panel	31.4 V
I_{SC}	Short circuit current PV panel	9.03 A
I_{mpp}	Maximum power point current PV panel	8.44 A
V_{coeff}	Voltage temperature coefficient PV panel	−0.31% K^{-1}
I_{coeff}	Current temperature coefficient PV panel	0.06% K^{-1}
W_{PV}	Weight PV panel	19 kg
C	Battery capacity	19.5 Ah
$T_{storage}$	Battery storage temperature	−40 to 60 °C
V_{rated}	Battery voltage rating	3.2 V
T_{op}	Battery operation temperature	−40 to 60 °C
$L_{battery}$	Battery length	22.7 cm
$W_{battery}$	Battery width	16 cm
$t_{battery}$	Battery thickness	0.725 cm
$L_{converter}$	Converter length	24.6 cm
$W_{converter}$	Converter width	26.6 cm
$t_{converter}$	Converter thickness	2.7 cm
t_{frame}	Frame thickness	2 mm
k_{glass}	Thermal conductivity of glass	1.38 W m^{-1} K^{-1}
k_{Si}	Thermal conductivity of Si	130 W m^{-1} K^{-1}
k_{eva}	Thermal conductivity of eva	0.38 W m^{-1} K^{-1}
k_{tedlar}	Thermal conductivity of tedlar	0.15 W m^{-1} K^{-1}
$k_{battery}$	Thermal conductivity of battery	0.81 W m^{-1} K^{-1}
k_{frame}	Thermal conductivity of frame	238 W m^{-1} K^{-1}
$c_{p,glass}$	Specific heat of glass	0.7 J g^{-1} K^{-1}
$c_{p,Si}$	Specific heat of Si	0.7 J g^{-1} K^{-1}
$c_{p,eva}$	Specific heat of eva	1.9 J g^{-1} K^{-1}
$c_{p,tedlar}$	Specific heat of tedlar	1.1 J g^{-1} K^{-1}
$c_{p,battery}$	Specific heat of battery	1.17 J g^{-1} K^{-1}
$c_{p,frame}$	Specific heat of frame	0.9 J g^{-1} K^{-1}
ρ_{glass}	Density of glass	2203 kg m^{-3}
ρ_{Si}	Density of Si	2329 kg m^{-3}
ρ_{eva}	Density of eva	930 kg m^{-3}
ρ_{tedlar}	Density of tedlar	1300 kg m^{-3}
$\rho_{battery}$	Density of battery	1965 kg m^{-3}
ρ_{frame}	Density of frame	2700 kg m^{-3}
ε_{glass}	Emissivity of glass	0.96
ε_{frame}	Emissivity of frame	0.77
ε_{tedlar}	Emissivity of tedlar	0.84
η_{PV}	Efficiency of PV panel	16.19%
g	acceleration of gravity	9.81 m s^{-2}
σ	Stefan–Boltzmann constant	5.67 × 10^{-8} W m^{-2} K^{-4}
R	Reflectivity at glass layer	7%
A	Absorptivity	3%

the surroundings for a particular geometry is convolute. As a consequence, an interface developed by COMSOL Multiphysics® is selected. This interface (conjugate heat transfer) interrelates and solves the differential equations that describe the heat transfer and the fluid flow mechanisms.

A 3D model is used in Sections 4.1 and 4.2, while in Sections 4.3 and 4.4 a 2D model was developed to reduce computation time. The 2D geometry had 52,203 elements, with 7420 boundary elements and average element quality of 0.85 for a triangular mesh. On the other hand, the quality of the elements was 0.7 for the 203,110 tetrahedral elements, from which 40,382 were at the boundaries.

3.1. Basic geometry

Fig. 2a presents a 2D layout of the integrated module, including the materials and layers of the proposed design. The features of the components are detailed in Tables 2 and 3, including the parameters and subscripts used in the equations.

3.2. Governing equations

3.2.1. Heat transfer in solids

The heat that is transferred by conduction is given by the diffusion equation as follows:

$$\nabla\cdot(k\nabla T) + \dot{q} = \rho c_p \frac{\partial T}{\partial t}, \tag{1}$$

where k is the thermal conductivity, T temperature vector, $\dot{q}$ heat generation, ρ density, c_p specific heat, and t time.

Eq. (1) is applied to the layers that compound the PV panel, the batteries, the charge controller, the microinverter, and the frame.

3.2.2. Heat transfer in fluids

Heat transfer in fluids occurs in the air domain, where it is defined as

$$\nabla\cdot(k\nabla T) + \dot{q} = \rho c_p \frac{\partial T}{\partial t} + \rho c_p (u\cdot\nabla T), \tag{2}$$

where u is the velocity of the fluid in all directions (x,y,z). In Eq. (2), the work produced by the pressure when the density is temperature dependent is neglected.

3.2.3. Fluid dynamics

The equations for momentum balance and continuity are used to model the fluid behaviour in the air domain, in order to obtain the velocity and pressure field. They are

$$\mu\nabla^2 u - \nabla p + F = \rho(u\cdot\nabla T) + \rho\frac{\partial u}{\partial t}, \tag{3}$$

$$\nabla\cdot u = 0, \tag{4}$$

where μ stands for viscosity, p for pressure in all directions, and F for fluid force. In the case of natural convection, the buoyant force produced by the fluid helps the heat dissipation. This force is calculated following Eq. (5), where a change in the density (ρ) of the fluid with respect to a reference point (ρ_{ref}) drives the phenomenon:

$$F = g(\rho - \rho_{ref}). \tag{5}$$

3.3. Coupling of physics

Eqs. (2) and (3) are completely coupled since both equations include the velocity term u. Moreover, properties like density and viscosity of the air are a function of pressure and temperature. Therefore, these two variables connect the heat transfer and fluid dynamics physics in a deeper manner.

3.4. Heat generation

The heat generated is assumed uniform for a given volume (3D model) or surface (2D model). In particular, this condition is applied to the following domains: battery, silicon layer, and glass domain layer.

3.4.1. PV panel

The irradiance (G) affects the glass layer and the silicon layer. The

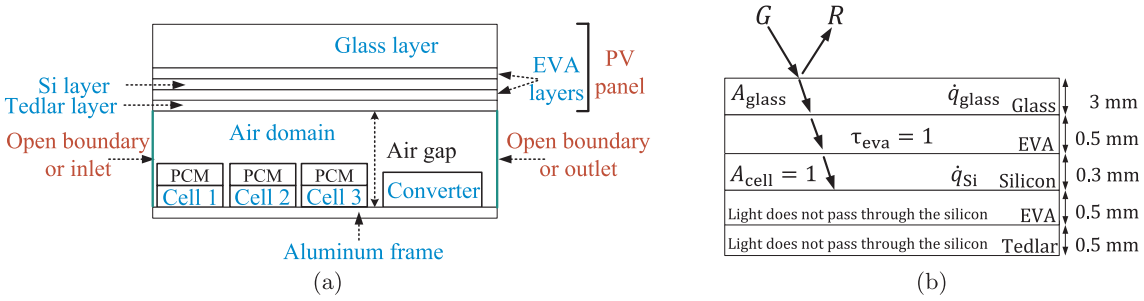

Fig. 2. (a) 2D layout of the integration concept, and (b) light interaction within the PV panel layers.

Table 3
Subscripts used in the FEM model.

Subscripts	Description
Glass	Property at glass layer
Si	Property at Silicon layer
PV	PV panel
Battery	Property at batteries
OC	Open circuit
Converter	Property at converter
In	Input
s	Surface
amb	Ambient
rad	Radiation
conv	Convection
ref	At reference point

incident light is partially reflected (R) at the glass surface (see Fig. 2b); then a portion of the remaining irradiance is absorbed by the glass (A_{glass}). All the irradiance from the glass is transmitted (A_{cell}) to the Si layer, where it is completely converted into heat, except the portion that produces electricity (η_{PV}). It is assumed that the eva layer and the tedlar layer do not interact with the incident light; hence, the heat generated in these layers is omitted.

The contribution of the heat generated in the glass layer and Si layer is calculated using the following:

$$\dot{q}_{glass} = \frac{G(1-R)A_{glass}}{t_{glass}}, \tag{6}$$

$$\dot{q}_{Si} = \frac{G(1-R)(1-A_{glass})(1-\eta_{PV})}{t_{Si}}. \tag{7}$$

3.4.2. Batteries

Battery heat generation equation accounts for the reversible and irreversible heat generation resulting from the charging and discharging processes. This heat can be calculated by using the following expression:

$$\dot{q}_{battery} = \frac{I}{V_{battery}}\left(V - V_{OC} + T\frac{\partial V_{OC}}{\partial T}\right). \tag{8}$$

where I is the charging or discharging current. The voltage (V) curve, open circuit voltage (V_{OC}) curve, and entropy coefficient ($\frac{\partial V_{OC}}{\partial T}$) are used according to the data provided by the manufacturer [33].

3.4.3. Converters

For the heat generating terms of the converters, the general approach is described by Eq. (9), where the instantaneous efficiency ($\eta_{converter}$) is taken from a look-up table that correlates power input (P_{in}) and power output, while $V_{converter}$ is the total volume of the converter:

$$\dot{q}_{converter} = \frac{P_{in}}{V_{converter}}(1-\eta_{converter}). \tag{9}$$

3.5. Boundary conditions

The predominance of either forced convection or natural convection results in different temperature values for the components. Therefore, different boundary conditions were applied to the FEM model to evaluate their influence.

Whereas for forced convection air enters (inlet) with a certain velocity at the left and leaves (outlet) at the right (Fig. 2a), for natural convection right and left boundaries are considered open-the air can enter or leave the domain.

3.5.1. Convection

Convection is used to include the effect of the surrounding air on the surfaces exposed to it. The heat transferred via convection was applied at the top of glass layer, and the bottom and sides of aluminium frame as follows:

$$q_{conv} = h(T_s - T_{amb}), \tag{10}$$

where T_s is the temperature of the boundary, T_{amb} ambient temperature, and h convection coefficient.

3.5.2. Radiation

The heat in form of radiation coming out of the top of the PV panel and the bottom of the aluminium frame is associated with the temperature of the body (T_s) and the temperature of the surroundings (T_{amb}):

$$q_{rad} = \sigma\varepsilon(T_s^4 - T_{amb}^4). \tag{11}$$

3.6. Inputs

Three days with the highest global horizontal irradiation (Fig. 3a), lowest wind velocity (Fig. 3b), and maximum ambient temperature (Fig. 3c) were chosen as inputs to the FEM model in Sections 4.3 and 4.4. Although it is very uncommon that the warmest day, least windy day, and the day with the highest irradiation coincide on the same day, this extreme scenario is defined as the most severe condition that the integrated device must handle due to high risk of components overheating. The data was taken from the Dutch Meteorological Institute (KMNI) at the Cesar Observatory (51.971°N, 4.927°E) throughout the year 2014, with a time resolution of 10 min.

3.6.1. Intermediate inputs

The battery system is driven by a simple control, where battery charging is a priority. The battery is charged according to the current produced by the PV panel which continuously varies, although it never surpasses 0.5 C-rate. After the sun stops shining and the battery is full, it is discharged at 0.25 C-rate (see Fig. 3d). The limits for charging are 90% state of charge (SoC) and 10% SoC when discharging, in order to protect the battery from overcharging or over-discharging, respectively. As can be seen in Fig. 3e, the heat generated during the charging process is negative, because of the undergoing endothermic process.

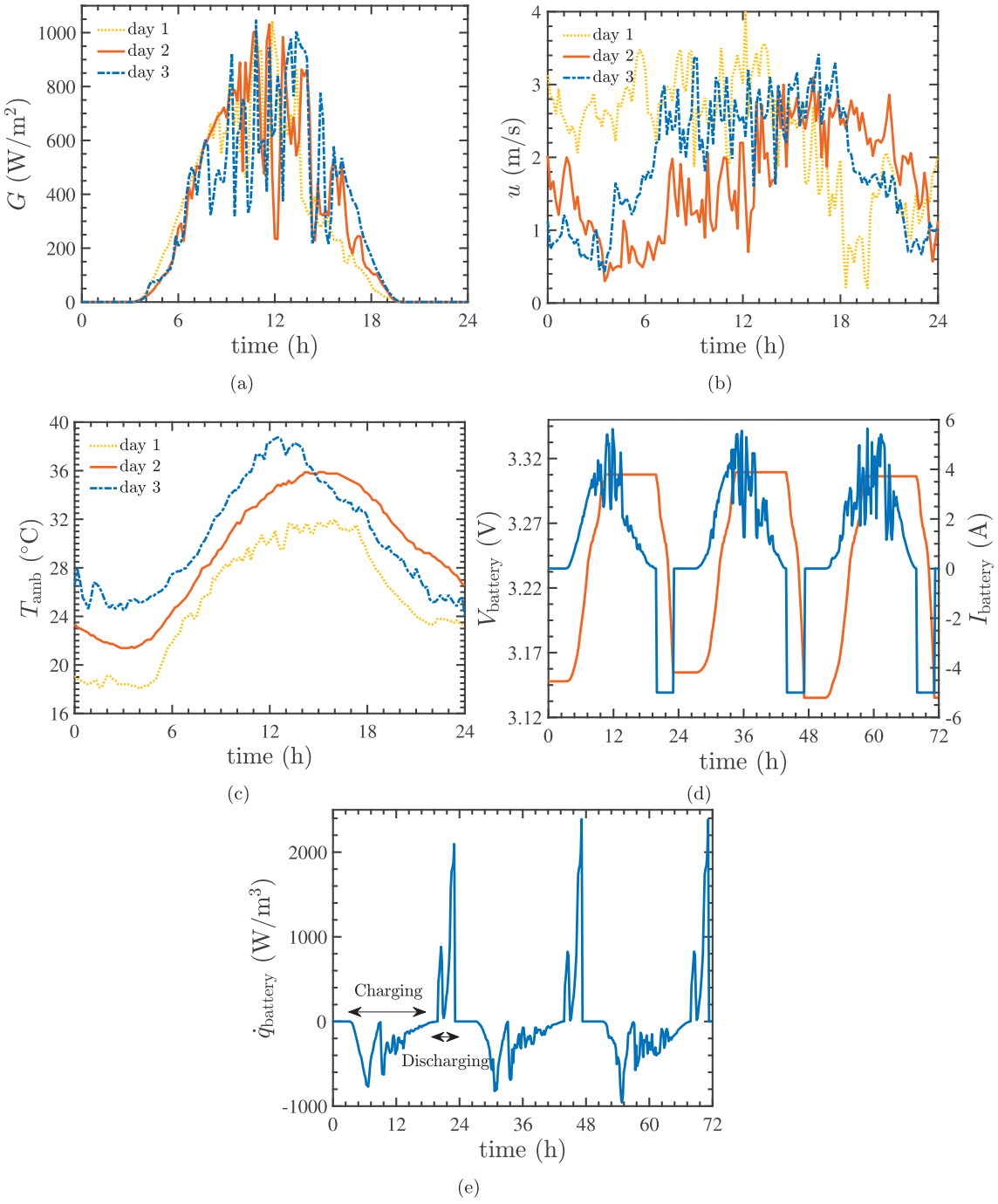

Fig. 3. Inputs to the FEM model for three days, (a) highest GHI, (b) lowest wind speed, (c) maximum ambient temperature, (d) cell voltage and current, and (e) heat generation in one cell.

Nevertheless, the battery pack releases heat to the surroundings when discharging.

The heat created inside the power electronics follows the pattern dictated by the solar irradiation. It is assumed that volume of the d.c./d.c. converter and microinverter are equal, but the moments at which the components act differ: the d.c./d.c. converter is on during charging, while the microconverter is active when discharging.

4. Results

4.1. Directly attached (DA) or not?

To achieve as compact *PBIM* as possible, attaching the components directly on the back side of the PV panel is an option. To evaluate this idea and compare to the non-attached (NA) case, the steady state model incorporates the parameters in Table 1. G is a high value of irradiation, while $\dot{q}_{\text{battery}}$ is the highest that can be generated at 1 C-rate when discharging. $\dot{q}_{\text{converter}}$ is calculated at the PV power production peak, whereas T_{amb} and h are considered appropriate in relation to the defined irradiance value. Moreover, forced convection is applied as shown in Fig. 2a varying the wind speed from 0.2 m s^{-1} up to 10 m s^{-1}, in order to understand its influence on the average temperatures of the devices.

The heat distribution in Fig. 4 shows that, for both NA and DA, the highest temperature is reached in the PV panel domain, due to the massive heat generated in the cell layer compared to the other heat sources. As a result, the temperature of the battery pack and converter are similar to the temperature of the PV panel for the DA case (see Fig. 4a and b).

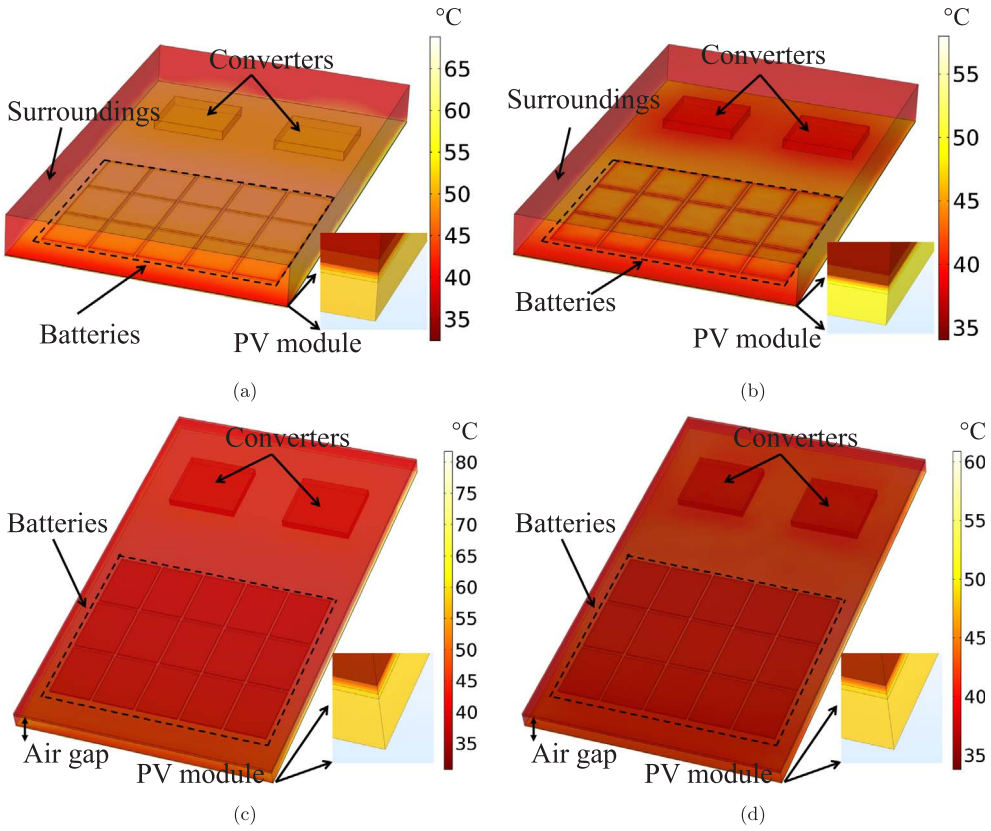

Fig. 4. Temperature distribution obtained from the FEM model: (a) directly attached and air velocity of 1 m s^{-1}, (b) directly attached and air velocity of 8 m s^{-1}, (c) air gap (50 mm) and air velocity of 1 m s^{-1}, (d) air gap (50 mm) and air velocity of 8 m s^{-1}. Note: in all the figures, the PV panel is facing down.

An increase in wind speed reduces the temperature of the components (Fig. 5a), while glass temperature is almost equal to the cell layer because of their proximity. In addition, the cooling effect of air is more pronounced on the converters than on the batteries, as the more extended area of the converter provides better heat dissipation.

By adding an air gap in between the PV panel and the components, the temperature of all components decreases considerably, since the air gap hinders the heat transfer from the PV panel to the other elements. Although increasing the wind speed helps remove heat from the components more efficiently when velocity increases, Fig. 5b also shows that at some point a further increase in wind velocity does not reduce the temperature of batteries and converters.

In the NA case, battery pack temperature depends on air speed, but mainly on the ambient temperature if the air gap is kept constant. Because according to Fig. 5c, the temperature of the battery increases with ambient temperature, 3 °C in this case.

4.2. Air gap

The air gap is the distance between the PV panel and the frame (see Fig. 2a), which is represented in the FEM model as the volume (or area) of the air domain. By increasing this domain, the temperature of the batteries and converters drop (Fig. 5d), although the air gap does not show a significant impact on the temperature of the PV panel (Fig. 5e).

Moreover, according to the battery and converter perspective, the optimal air gap thickness varies from 5 cm to 7 cm. Increasing its thickness more than 7 cm does not reduce the temperature of the components, but it may rather augment the volume/weight ratio, which should be kept as low as possible.

4.3. Natural and forced convection

In this section, the data described in Section 3.6 is employed by a transient model to incorporate the effect of the environmental conditions that the *PBIM* could face in an extreme scenario.

As expected, the temperature of PV cells rises with poor cooling conditions. With natural convection as a dominant phenomenon, the temperatures can increase 10 °C more than in the case where forced convection is the primary cooling mechanism (see Fig. 6a). In this figure, the benchmark dictates the minimum temperatures for a PV panel without any device attached.

Battery temperature does not differ significantly when either under forced convection or natural convection as the dominant mechanism, as Fig. 6b suggests. However, a minor reduction is observed for the forced convection case.

Batteries operate within a safe range, because even under harsh conditions the battery temperature never surpasses 39 °C (third day for natural convection conditions), which is under the defined maximum temperature of operation: 60 °C ([33]).

According to Fig. 6a and b, the temperature of the batteries and PV cell do not follow the same pattern. PV cell temperature responds mainly to irradiance and ambient temperature, while batteries respond to ambient temperature. The effect of ambient temperature on battery temperature is more important, even if the battery discharges at a relatively high C-rate (0.5 C), as the amount of heat produced by the battery is overshadowed by the heat coming from the surroundings. Of course, this applies as long as the batteries are neither overcharged nor over-discharged.

4.4. Phase change materials

Even though it has been demonstrated that batteries do not surpass the upper-temperature limit defined by the manufacturer, the operating temperature must be kept as low as possible to prevent accelerated battery ageing and thermal runway [34,35].

PCM are proposed as a passive cooling method, since forced convection is unable to diminish the temperature of the batteries significantly. PCM materials store thermal energy not allowing battery

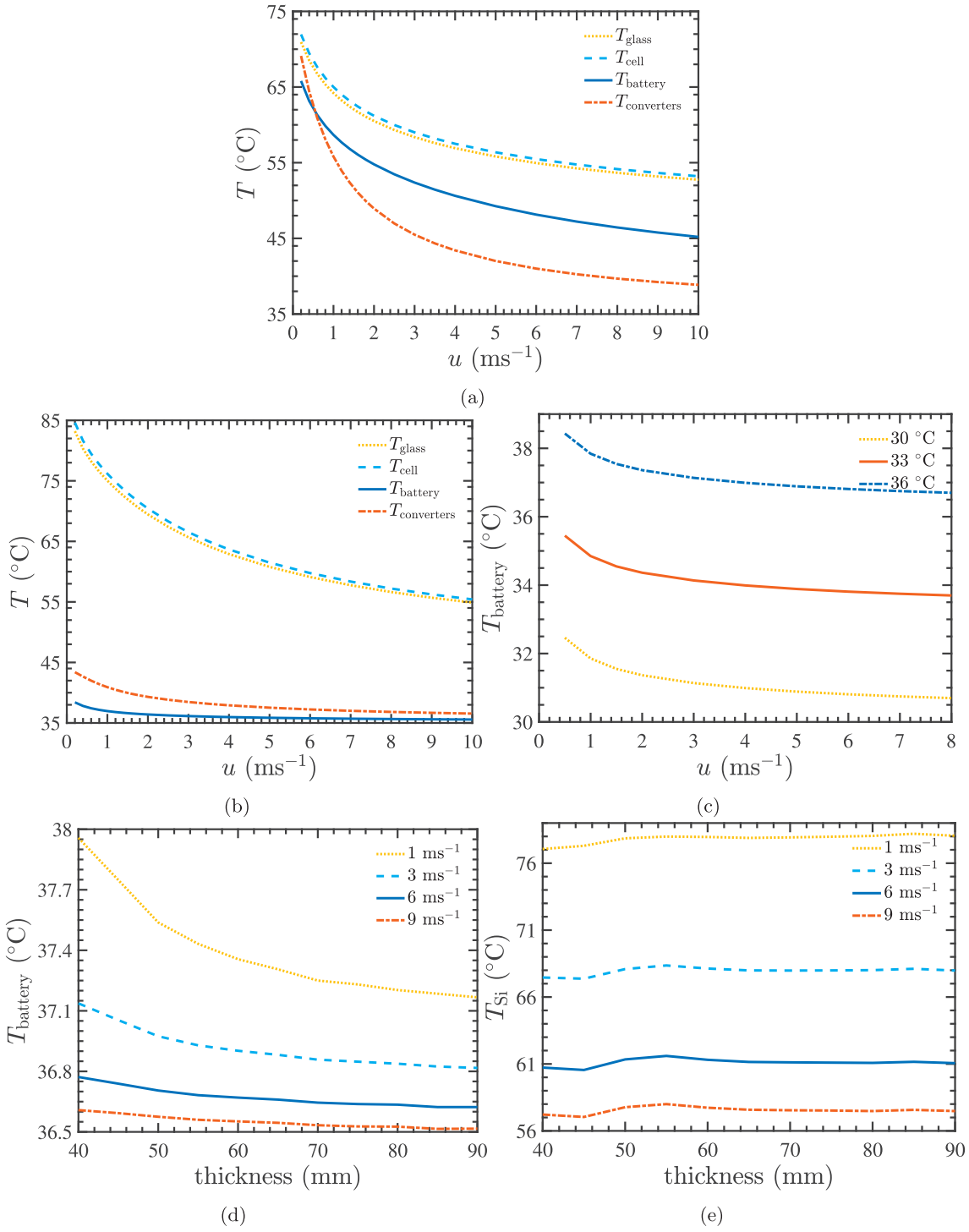

Fig. 5. Temperature obtained from the FEM model: (a) components when directly attached, (b) components when not attached (air gap of 50 mm), (c) battery at different ambient temperatures (30 °C, 33 °C, and 36 °C) for an air gap of 50 mm, (d) battery for various air gaps and air velocities, and (e) Si layer average for different air gaps and velocities.

temperature to increase fast; they also maintain $T_{battery}$ under a specific value as long as PCM does not saturate.

To study the effect of PCM over $T_{battery}$ a layer of PCM is placed at the top of batteries (Fig. 2a). The PCM used has a thickness of 5 mm, a density of 900 kg/m^3, a thermal conductivity of 5 W m^{-1} K^{-1}, a phase change temperature range (ΔT) of 6 °C, and a heat capacity of 1.9 J g^{-1} K^{-1} when solid and 2.3 J g^{-1} K^{-1} when liquid. Only the latent heat (L), phase change temperature (T_{PC}), and thickness are modified to perform a parametric analysis later on.

As can be seen in Fig. 6b, a PCM with a phase change (PC) temperature of 36 °C and L of 250 J g^{-1} shaves the third-day temperature peak by 3 °C, and to a smaller extent the second-day peak. In case the latent heat increases from 250 J g^{-1} to 300 J g^{-1}, for a T_{PC} of 36 °C, the temperature of the batteries does not drop because the phase changing process starts later. Also in Fig. 6b, the results show that $T_{battery}$ reduces for a T_{PC} of 34 °C and L of 250 J g^{-1}, where the second peak and third peak are shaved better. Since the PC process starts at around 30 °C and finishes near 36 °C, the reduction of battery temperature intensifies because more heat it is absorbed than in the other cases.

To reduce $T_{battery}$ even further, either PCM thickness or L might be

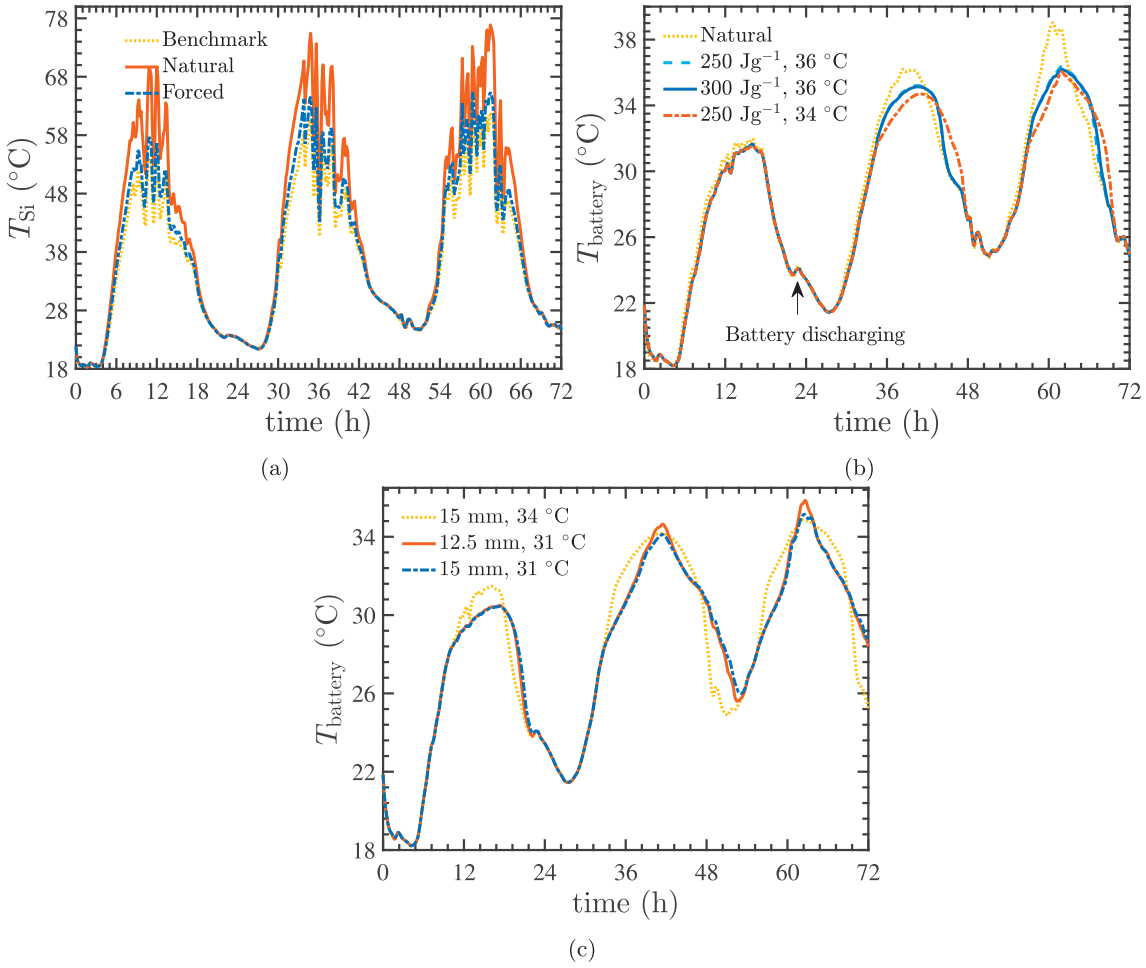

Fig. 6. (a) Average Si layer temperature for natural and forced convection (50 mm air gap), (b) average battery temperature for forced convection, natural convection, and different PCM (5 mm thick), and (c) average battery temperature for various PCM thickness and PC temperatures.

increased, both for lower T_{PC}. However, a L of 250 J g^{-1} is already high for the existing PCM. Hence, just the thickness varies as follows.

The effect of increasing the thickness for two phase change temperatures is illustrated in Fig. 6c, indicating that a PCM with a T_{PC} of 31 °C and 12.5 mm thick is able to shave all the three peaks, although as expected, 15 mm thick PCM has better results for the second and third peaks. However, a PCM with a T_{PC} of 34 °C and a thickness of 15 mm is not capable of shaving the first peak, which indicates that this combination is not a candidate for the final design of the *PBIM*. Finally, a 15 mm PCM with a T_{PC} of 31 °C is the overall best option. Due to its performance at elevated temperatures, but also when temperatures are not extremely high; which is usually the case for *PBIM* on a daily basis.

5. Validation of the FEM model

A prototype was built and tested to validate the FEM model. The validation was carried out comparing the outcomes of the model and experimental measurements, using the same initial and boundary conditions. The testing set up, the characteristics of the prototype, and the results of the comparison are described as follows.

5.1. Testing set-up

A 30 W_p PV panel from Blue Solar was connected to a Genasun GV-5-Li-14.2V charge controller which performs maximum power point tracking. The charge controller imposes a constant current and constant voltage profile during the battery charging process. Moreover, four batteries with a capacity of 8 Ah and a nominal voltage of 3.2 V (WN08AH) were connected to the charge controller and a 10 Ω load (See Fig. 7a). Before testing, two thermocouples were attached to the top and back side of a selected battery, while another thermocouple was placed at the upper part of the PV panel. All temperature measurements were taken with a time resolution of 5 min.

After connecting all the components and measuring devices, the prototype was placed under a small solar simulator (0.6 × 0.5 m) that produces a constant radiation of 900 W m^{-2}, while the ambient temperature was around 25 °C during the test. Fig. 7c and b show the spatial arrangement of the components and the prototype under testing, respectively.

At the beginning of the test, the batteries are partially charged (90% SoC), and as the test continues they are charged at a constant current of 1.65 A.

5.2. Results

After one hour of testing, the temperature of the batteries reached steady state condition, as can be observed in Fig. 7d. The measured temperature at the bottom and top of batteries corresponds to the values predicted by the FEM model.

The temperature of the PV panel increased up to 70 °C, as expected in the FEM model and the IR image in Fig. 7e. The steady state time for the PV panel is around 40 min, considerably lower than that for the batteries. This mismatch occurs, first, because the heat from the PV panel is conducted to the aluminium frame and then to the batteries, taking some time to be transferred. And secondly, because the air where the components were placed is heated up gradually, creating an

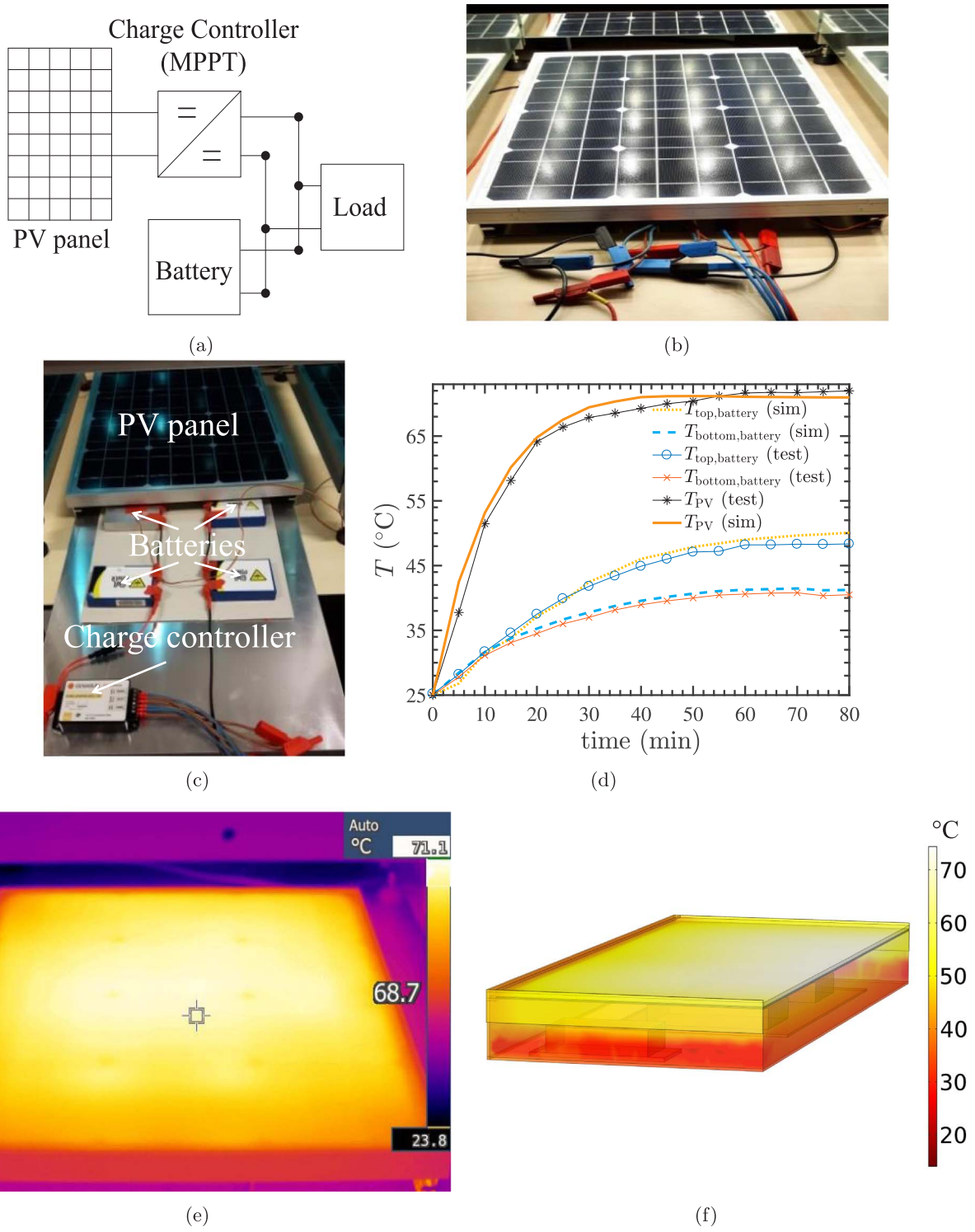

Fig. 7. (a) Electric diagram of the prototype, (b) prototype under testing, (c) components of the prototype, (d) temperature of the components according to simulation (sim) and lab measurements (test), (e) temperature distribution at the top of the PV panel instants before finishing the test (IR image), and (f) simulation results of FEM model.

equilibrium temperature more slowly compared to the PV panel.

Future research must be done to understand the impact of elevated temperatures in the performance of the integrated module, in order to understand, for instance, how ageing decreases battery lifetime, and state of health.

6. Conclusion

A FEM model was developed and validated testing a prototype to study the thermal behaviour of the PV-Battery Integrated Module. The model shows that directly attaching the components at the back of the solar panel results in extreme temperatures for the battery pack, suggesting the necessity of an air gap between them. The air gap helps to reduce the temperature of the components, impeding the heat generated at the PV panel from warming the batteries and converters. The optimal air gap is between 5 and 7 cm, in order to provide an appropriate packaging/cooling ratio.

Even under severe conditions, maximum battery temperature never

surpassed 39 °C. This temperature is lower than the maximum temperature of operation defined by the manufacturer. However, because convection has a limited effect in decreasing the temperature of the components, phase change materials are proposed as a passive cooling method. Phase change materials prove to be useful for shaving battery temperature peaks, reducing the maximum battery temperature by 5 °C.

In summary, the battery pack operates in a safe range, confirming the feasibility of the *PBIM* concept as a future solution for solar-battery systems.

Acknowledgment

This work is financially supported by the Universidad de Costa Rica, Ministerio de Ciencia y Tecnología y Telecomunicaciones of Costa Rica, and Consejo Nacional para Investigaciones Científicas y Tecnológicas. The authors thank Nishant Narayan and Novy Francis.

References

[1] Jäger-waldau A. PV status report 2016, No. October; 2016. doi:http://dx.doi.org/10.2790/749737.
[2] Nykvist B, Nilsson M. Rapidly falling costs of battery packs for electric vehicles. Nat Clim Change 2015;5(April):329–32. http://dx.doi.org/10.1038/nclimate2564.
[3] Fu R, Chung D, Lowder T, Feldman D, Ardani K, Fu R, et al. U.S. solar photovoltaic system cost benchmark: Q1 2016, Nrel/Tp-6a20-66532 (September). < http://www.nrel.gov/docs/fy15osti/64746.pdf > .
[4] Vega-Garita V, Harsarapama AP, Ramirez-Elizondo L, Bauer P. Physical integration of PV-battery system: Advantages, challenges, and thermal model. In: 2016 IEEE international energy conference, ENERGYCON; 2016. doi:http://dx.doi.org/10.1109/ENERGYCON.2016.7514038.
[5] Rand BP, Genoe J, Heremans P, Poortmans J. Solar cells utilizing small molecular weight organic semiconductors. Prog Photovolt: Res Appl 2007;15(February 2013):659–76. http://dx.doi.org/10.1002/pip.1160. Available from: arXiv:1303.4604.
[6] Raffaelle RP, Hepp AF, Landis GA, Hoffman DJ. Mission applicability assessment of integrated power components and systems. Prog Photovolt: Res Appl 2002;10(6):391–7. http://dx.doi.org/10.1002/pip.445.
[7] Lee Y-H, Kim J-S, Noh J, Lee I, Kim HJ, Choi S, et al. Wearable textile battery rechargeable by solar energy. Nano Lett 2013;13(11):5753–61. http://dx.doi.org/10.1021/nl403860k. [pMID: 24164580].
[8] Jost K, Dion G, Gogotsi Y. Textile energy storage in perspective. J Mater Chem A 2014;2(28):10776. http://dx.doi.org/10.1039/c4ta00203b<http://xlink.rsc.org/?DOI=c4ta00203b>.
[9] Ostfeld AE, Gaikwad AM, Khan Y, Arias AC. High-performance flexible energy storage and harvesting system for wearable electronics. Sci Rep 2016;6(April):26122. http://dx.doi.org/10.1038/srep26122. < https://doi.org/10.1038/srep26122%5Cnhttp://www.nature.com/articles/srep26122 > .
[10] Song T, Sun B. Towards photo-rechargeable textiles integrating power conversion and energy storage functions: can we kill two birds with one stone? ChemSusChem 2013;6(3):408–10. http://dx.doi.org/10.1002/cssc.201200889.
[11] Lv T, Yao Y, Li N, Chen T. Wearable fiber-shaped energy conversion and storage devices based on aligned carbon nanotubes. Nano Today 2016;11(5):644–60. http://dx.doi.org/10.1016/j.nantod.2016.08.010.
[12] Zhai S, Karahan HE, Wei L, Qian Q, Harris AT, Minett AI, et al. Textile energy storage: structural design concepts, material selection and future perspectives. Energy Storage Mater 2016;3:123–39. http://dx.doi.org/10.1016/j.ensm.2016.02.003.
[13] Wang X, Jiang K, Shen G. Flexible fiber energy storage and integrated devices: recent progress and perspectives. Mater Today 2015;18(5):265–72. http://dx.doi.org/10.1016/j.mattod.2015.01.002.
[14] Guo W, Xue X, Wang S, Lin C, Wang ZL. An integrated power pack of dye-sensitized solar cell and Li battery based on double-sided TiO2 nanotube arrays. Nano Lett 2012;12:2520–3. http://dx.doi.org/10.1021/nl3007159.
[15] Agbo SN, Merdzhanova T, Yu S, Tempel H, Kungl H, Eichel RA, et al. Development towards cell-to-cell monolithic integration of a thin-film solar cell and lithium-ion accumulator. J Power Sour 2016;327:340–4. http://dx.doi.org/10.1016/j.jpowsour.2016.07.073.
[16] Krebs FC, Fyenbo J, Jørgensen M. Product integration of compact roll-to-roll processed polymer solar cell modules: methods and manufacture using flexographic printing, slot-die coating and rotary screen printing. J Mater Chem 2010;20(41):8994. http://dx.doi.org/10.1039/c0jm01178a.
[17] Xie K, Wei B. Materials and structures for stretchable energy storage and conversion devices. Adv Mater 2014;26(22):3592–617. http://dx.doi.org/10.1002/adma.201305919.
[18] Wills RH, Krauthamer S, Bulawka A, Posbic JP. The AC photovoltaic module concept. In: Proceedings of the 32nd intersociety energy conversion engineering conference (IECEC); 1997. p. 1562–3. doi:http://dx.doi.org/10.1109/IECEC.1997.656653.
[19] Ačanski M, Popović-Gerber J, Ferreira B. Thermal modeling of the module integrated DC-DC converter for thin-film PV modules. In: Proceedings of EPE-PEMC 2010 - 14th international power electronics and motion control conference; 2010. p. 160–65. doi:http://dx.doi.org/10.1109/EPEPEMC.2010.5606523.
[20] Reynaud JF, Alonso C, Aloisi P, Cabal C, Estibals B, Rigobert G, et al. Multifunctional module lithium-ion storage and photovoltaic conversion of solar energy. In: Conference record of the IEEE photovoltaic specialists conference; 2008. pp. 1–5. doi: http://dx.doi.org/10.1109/PVSC.2008.4922836.
[21] Reynaud JF, Gantet O, Aloïsi P, Estibals B, Alonso C. New adaptive supervision unit to manage photovoltaic batteries. In: IECON proceedings (industrial electronics conference); 2009. p. 664–9. doi:http://dx.doi.org/10.1109/IECON.2009.5414999.
[22] Reynaud JF, Gantet O, Aloïsi P, Estibals B, Alonso C. A novel distributed photovoltaic power architecture using advanced Li-ion batteries. In: Proceedings of EPE-PEMC 2010 - 14th international power electronics and motion control conference; 2010. p. 6–12. doi:http://dx.doi.org/10.1109/EPEPEMC.2010.5606548.
[23] Grzesiak W, Mackow P, Maj T, Polak A, Klugmann-Radziemska E, Zawora S, et al. Innovative system for energy collection and management integrated within a photovoltaic module. Solar Energy 2016;132:442–52. http://dx.doi.org/10.1016/j.solener.2016.03.043.
[24] Sarhaddi F, Farahat S, Ajam H, Behzadmehr A, Mahdavi Adeli M. An improved thermal and electrical model for a solar photovoltaic thermal (PV/T) air collector. Appl Energy 2010;87(7):2328–39. http://dx.doi.org/10.1016/j.apenergy.2010.01.001.
[25] Tiwari GN, Mishra RK, Solanki SC. Photovoltaic modules and their applications: a review on thermal modelling. Appl Energy 2011;88(7):2287–304. http://dx.doi.org/10.1016/j.apenergy.2011.01.005.
[26] Wang Q, Jiang B, Li B, Yan Y. A critical review of thermal management models and solutions of lithium-ion batteries for the development of pure electric vehicles. Renew Sust Energy Rev 2016;64:106–28. http://dx.doi.org/10.1016/j.rser.2016.05.033.
[27] Monu M, Ibrahim D, Rosen Ma. Review on use of phase change materials in battery thermal management for electric and hybrid electric vehicles. Int J Energy Res 2016;40(8):1011–31. http://dx.doi.org/10.1002/er. Available from: arXiv:1011.1669v3.
[28] Ling Z, Zhang Z, Shi G, Fang X, Wang L, Gao X, et al. Review on thermal management systems using phase change materials for electronic components, Li-ion batteries and photovoltaic modules. Renew Sust Energy Rev 2014;31:427–38. http://dx.doi.org/10.1016/j.rser.2013.12.017.
[29] Javani N, Dincer I, Naterer GF, Yilbas BS. Heat transfer and thermal management with PCMs in a Li-ion battery cell for electric vehicles. Int J Heat Mass Transfer 2014;72:690–703. http://dx.doi.org/10.1016/j.ijheatmasstransfer.2013.12.076.
[30] Ling Z, Chen J, Fang X, Zhang Z, Xu T, Gao X, et al. Experimental and numerical investigation of the application of phase change materials in a simulative power batteries thermal management system. Appl Energy 2014;121:104–13. http://dx.doi.org/10.1016/j.apenergy.2014.01.075.
[31] Wang H, Wang F, Li Z, Tang Y, Yu B, Yuan W. Experimental investigation on the thermal performance of a heat sink filled with porous metal fiber sintered felt/paraffin composite phase change material. Appl Energy 2016;176:221–32. http://dx.doi.org/10.1016/j.apenergy.2016.05.050.
[32] Qu ZG, Li WQ, Tao WQ. Numerical model of the passive thermal management system for high-power lithium ion battery by using porous metal foam saturated with phase change material. Int J Hydrogen Energy 2014;39(8):3904–13. http://dx.doi.org/10.1016/j.ijhydene.2013.12.136.
[33] A123 systems, battery pack design, validation, and assembly guide using A123 systems AMP20M1HD-A nanophosphate cells; 2014. p. 1–71. < http://www.formula-hybrid.org/wp-content/uploads/A123_AMP20_battery_Design_guide.pdf > .
[34] Palacin MR, de Guibert A. Why do batteries fail? Science 2016;351(6273). http://dx.doi.org/10.1126/science.1253292. 1253292-1253292 <http://www.sciencemag.org/cgi/doi/10.1126/science.1253292>.
[35] Feng X, Sun J, Ouyang M, He X, Lu L, Han X, et al. Characterization of large format lithium ion battery exposed to extremely high temperature. J Power Sour 2014;272:457–67. http://dx.doi.org/10.1016/j.jpowsour.2014.08.094.